Simultaneous infrared observations of the Jovian auroral ionosphere and thermosphere

Wang, R., Stallard, T. S., Melin, H., Baines, K. H., Moore, L., O'Donoghue, J. ORCID: https://orcid.org/0000-0002-4218-1191, Johnson, R. E., Thomas, E. M., Knowles, K. L., Tiranti, P. I. and Miller, S. (2024) Simultaneous infrared observations of the Jovian auroral ionosphere and thermosphere. Journal of Geophysical Research: Space Physics, 129 (12). e2024JA032891. ISSN 2169-9402 doi: 10.1029/2024JA032891 Available at https://centaur.reading.ac.uk/120067/

To link to this article DOI: http://dx.doi.org/10.1029/2024JA032891

Publisher: American Geophysical Union

JGR Space Physics

RESEARCH ARTICLE

10.1029/2024JA032891

Key Points:

- Scanning maps of H_3^+ radiance, temperature, column density, and H_2 radiance are produced using Keck-NIRSPEC
- Correlations between derived quantities are investigated to study the heating mechanism of Jupiter's auroral thermosphere
- The source of heating may originate from an altitude between the stratosphere and H_3^+ overtone and H_2 emission peak altitudes

Correspondence to:

R. Wang,
rw318@leicester.ac.uk

Citation:

Wang, R., Stallard, T. S., Melin, H., Baines, K. H., Moore, L., O'Donoghue, J., et al. (2024). Simultaneous infrared observations of the Jovian auroral ionosphere and thermosphere. *Journal of Geophysical Research: Space Physics*, *129*, e2024JA032891. https://doi.org/10.1029/2024JA032891

Received 17 MAY 2024
Accepted 21 NOV 2024

Simultaneous Infrared Observations of the Jovian Auroral Ionosphere and Thermosphere

Ruoyan Wang[1], Tom S. Stallard[2], Henrik Melin[2], Kevin H. Baines[3,4], Luke Moore[5], James O'Donoghue[6], Rosie E. Johnson[7], Emma M. Thomas[2], Katie L. Knowles[2], Paola I. Tiranti[2], and Steve Miller[8]

[1]School of Physics and Astronomy, University of Leicester, Leicester, UK, [2]Department of Mathematics, Physics and Electrical Engineering, Northumbria University, Newcastle upon Tyne, UK, [3]Jet Propulsion Laboratory, California Institute of Technology, Pasadena, CA, USA, [4]Space Science and Engineering Center, University of Wisconsin-Madison, Madison, WI, USA, [5]Center for Space Physics, Boston University, Boston, MA, USA, [6]Department of Meteorology, University of Reading, Reading, UK, [7]Department of Physics, Aberystwyth University, Aberystwyth, UK, [8]Department of Physics and Astronomy, University College London, London, UK

Abstract Simultaneous observations of H_3^+ and H_2 in Jupiter's northern infrared aurora were conducted on 02 June 2017 using Keck-NIRSPEC to produce polar projection maps of H_3^+ radiance, rotational temperature, column density, and H_2 radiance. The temperature variations within the auroral region are $\sim 700 - 1000$ K, generally consistent with previous studies, albeit with some structural differences. Known auroral heating sources including particle precipitation, Joule heating, and ion drag have been examined by studying the correlations between each derived quantity, yet no single dominant mechanism can be identified as the main driver for the energetics in Jupiter's northern auroral region. It appears that a complex interaction exists between the heating driven by various mechanisms and the cooling from the H_3^+ thermostat effect. Comparisons between the H_3^+ temperature and the line-of-sight ion velocity in the reference frame of (a) the planetary rotation and (b) the neutral atmosphere further suggest that the local thermodynamic equilibrium effect may play an important role in thermospheric heating at Jupiter. Along with previously reported heating events that occurred in both the lower and upper atmosphere, it is speculated that the heating source may originate from an altitude above Jupiter's stratosphere but below the peak altitude of H_3^+ overtone and H_2 quadrupole emissions.

1. Introduction

Since the discovery of H_3^+ on Jupiter (Drossart et al., 1989), it has long been used to probe the upper atmospheric chemistry, energetics, and dynamics of giant planets, as well as the magnetosphere-ionosphere-thermosphere coupling processes. Searching for temperature variations in H_3^+ has been one of the main focuses of spectroscopic studies (see the review by Miller et al., 2020, and references therein). Despite many attempts over the years, mechanisms behind the heating and cooling of the Jovian thermosphere remain ambiguous. The interaction between Jupiter's upper atmosphere and magnetosphere, through energetic particle precipitations (Grodent et al., 2001; Yelle & Miller, 2004), Joule heating (Millward et al., 2005; Smith et al., 2005), and ion drag (Miller et al., 2000; Millward et al., 2005; Smith et al., 2005), has been thought to be one of the major causes of thermospheric heating at Jupiter. Joule heating refers to the thermalized kinetic energy that heats the atmosphere, and ion drag is the result of an exchange of kinetic energy between neutral and ionized gases, both of which stem from relative motions between the two components (Smith et al., 2005; Vasyliūnas & Song, 2005). Measurements of H_3^+ temperature can be used to infer the thermospheric temperature, as these ions are considered to be in quasi-local thermodynamic equilibrium local thermodynamic equilibrium (LTE) with the surrounding neutral atmosphere (e.g., Melin et al., 2005; Miller et al., 2000; Tao et al., 2011). Spectroscopic infrared observations of Jupiter's aurora have reported H_3^+ ion velocity, temperature, density, and emission intensities (e.g., Chaufray et al., 2011; Johnson et al., 2017, 2018; Moore et al., 2017; Raynaud et al., 2004; Stallard et al., 2001, 2002). Recent works using instruments with higher spatial and spectral resolution have produced auroral, polar, and even global mappings (e.g., Adriani et al., 2017; Moore et al., 2017; O'Donoghue et al., 2021). An approach to investigate particle precipitation, Joule heating, and ion drag as potential heating mechanisms is thus to compare the physical quantities measured directly from the observed H_3^+ emissions (Johnson et al., 2018; Raynaud et al., 2004).

Direct measurements of H_2 emission intensity, temperature, and column density allow investigations of the physical and chemical mechanisms that cause the structural changes and dynamics of Jupiter's thermosphere. The near-infrared provides a unique window for investigating auroral emissions at high latitudes. Within the atmospheric K-band window ($\sim 1.9 - 2.5\ \mu m$), several prominent H_2 quadrupole lines and multiple H_3^+ overtone lines span, suggesting the viability of probing infrared auroral emissions from both neutrals and plasmas using K-band spectroscopy. Theoretically, it is possible to perform analogous studies on the infrared quadrupole lines of H_2 as on H_3^+ emission lines (Trafton et al., 1989), but such studies have been very limited in the past. Kim et al. (1990) measured the rotational temperature of $\sim$540–1,230 K from H_2 $S_1(0)$, $S_1(1)$, and $S_1(2)$ lines in the southern aurora with notable large error bars. The main challenge of data processing is the relatively low signal-to-noise ratio, primarily due to uncertainties associated with instrumental effects and background noise.

Raynaud et al. (2004) observed the auroral emission of Jupiter near 2.1 μm and managed to capture the H_2 $S_1(1)$ quadrupole line with several H_3^+ overtone lines, which allow them to map the emission distribution of H_2. The thermospheric temperature and density could not be measured due to insufficient H_2 lines. With the same data, Chaufray et al. (2011) determined the thermospheric wind velocity of <1.0 km/s; only the upper limit can be constrained due to large uncertainties. Wang et al. (2023) conducted another simultaneous observation in the K band and observed the H_3^+ and H_2 emission lines, from which the authors derived the line-of-sight Doppler shift velocities of ion and neutral winds. Their result revealed subcorotational neutral velocities within the auroral region, showing that Jupiter's thermosphere departs from corotating with the internal rotation of the planet. Consequently, it is important to account for the neutral components when examining the correlations between thermospheric temperature and ion wind velocities. Previous measurements of vertical distributions have found that the peak H_3^+ overtone and H_2 quadrupole emissions share the same altitudinal range at $\sim 700 - 900$ km in the Jovian upper atmosphere (Kita et al., 2018; Uno et al., 2014). Under these circumstances, Wang et al. (2023) calculated the relative velocity between H_2 and H_3^+, that is, the ion wind in the context of the neutral atmosphere, defined as the effective ion drift. With the thermospheric wind velocity considered, the effective ion drift may be a more accurate indicator of ion-neutral interactions in Jupiter's upper atmosphere.

We present here spatial maps of H_3^+ radiance, temperature, and column density, along with the H_2 radiance, obtained from a high-resolution simultaneous observation of Jupiter's northern aurora. On top of this, we analyze the correlations within these parameters and between the effective ion drift derived in Wang et al. (2023) to investigate the heating mechanism of the auroral thermosphere. Details of the observation and data reduction are described in Section 2. Polar maps of the ion and neutral parameters are provided in Section 3. The results are discussed in Section 4, followed by the conclusion in Section 5.

2. Observation and Data Processing

The observation was conducted on 02 June 2017 from 06:23 to 07:40 UTC, using the NIRSPEC instrument on the Keck II telescope. Jupiter's northern aurora was scanned twice from the pole toward the equator with an east-west slit of size $0.288 \times 24''$ and a step size of $0.2''$. The wavelength range of the instrument is set to the K band, aiming at $\sim 2.062 - 2.416\ \mu m$ in the near-infrared, allowing for simultaneous observations of H_2 quadrupole and H_3^+ overtone emission lines. Positions of the echelle and the cross-disperser were set to 63.9 and 35.6, respectively. The weather was clear and stable throughout the night, with the average air mass measured at $\sim$1.1 and the seeing recorded as $\sim 0.6''$. Jupiter's equatorial diameter at the time of observation was $\sim 40.6''$, with a sub-Earth latitude of ~ -3.098 degrees. A total of 38 spectral images, excluding calibration exposures and sky frames, were obtained by combining six integrations, each 10 s long. Table 1 summarizes the H_3^+ overtone and H_2 quadrupole emission lines used for analysis, all from echelle order 32 (2.382–2.416 μm) and order 36 (2.117–2.148 μm).

An open-source Python package `h3ppy` is used to derive the H_3^+ radiance, rotational temperature, and column density. Figure 1 shows an example of the observed spectra and model fits, attached with the derived rotational temperature and column density. Gaussian fits are performed to the H_2 spectra as in Wang et al. (2023) to retrieve the H_2 radiance. The resultant scanning maps are polar projected into jovigraphic coordinates by identifying the slit position relative to the locations of the limb of Jupiter in the slit-viewing camera image. The planetary limb can be determined using the Jovian polar flattening, the sub-Earth latitude of the telescope, and the central meridian longitude. The calculated limb is then used to assign latitude and longitude to each spatial and spectral pixel onto a 360×180 degree grid with a bin size of 1°. The limb brightening effect is removed from calculations

Table 1
Spectroscopic Properties of H_3^+ *and* H_2 *Lines Used for Analysis*

Order	Assign.	λ (μm)	ν_2	J_{upper}	ω_{upper} (cm^{-1})	ω (cm^{-1})	A_{if} (s^{-1})	g_{ns}
36	Q(5,2)	2.1221	2–0	5	5835.27	4712.29	67.04	2
36	P(4,1)	2.1277	2–0	3	5469.61	4700.15	56.44	2
36	Q(4,2)	2.1314	2–0	4	5396.33	4691.98	58.93	2
36	R(8,8)	2.1343	2–0	9	6269.9	4686.76	161.8	8/3
36	Q(3,2)	2.1380	2–0	3	5041.16	4677.27	42.06	2
36	P(3,0)	2.1439	2–0	2	5117.06	4664.3	63.76	4
36	$S_1(1)$	2.1220	1–0	3	6951.3	4712.9	3.47	21
32	$Q_1(1)^*$	2.4066	1–0	1	6149.0	4155.25	4.294	9
32	$Q_1(2)^*$	2.4134	1–0	2	6471.4	4143.5	3.051	5

Note. The lines with an asterisk are associated with large uncertainties (discussed in detail in the Results section). References of the line list are Neale et al. (1996) and Roueff et al. (2019).

of radiance and column density (correction not needed for temperature due to the same variation in the radiance used for calculation, under the assumption of uniformity), following the same method as in Johnson et al. (2017).

3. Results

Figure 2 shows the main results of this study: scanning maps of H_3^+ radiance, rotational temperature, column density, and H_2 radiance. Figures 2a–2d refer to the first scan and Figures 2e–2h to the second scan, with the latter covering a larger region toward the middle latitude. The H_3^+ radiance shown in Figures 2a and 2e have the mean values of 0.36 and 0.28 μWm^{-2}sr^{-1}, respectively, which are of the same order of magnitude as the H_3^+ overtone profiles in Kita et al. (2018). The main emission is sharp on the dawn side and more expanded on the dusk side, bright along the auroral peak of the Grodent et al. (2001) model in both sectors. Additionally, a large dark spot is seen in the polar region at ∼60°N, 180°. These features broadly agree with the projected radiance map of H_3^+ overtone emissions in Raynaud et al. (2004) and fundamental emissions in Moore et al. (2017) and Johnson et al. (2018).

The derived H_3^+ rotational temperatures shown in Figures 2b and 2f range approximately between 700 and 1,000 K, with mean values of 892 and 849 K, which are in agreement with previous measurements. Along the auroral peaks, two high-temperature regions are found near 60°N, 165°E and 65°N, 150°W, along with a large

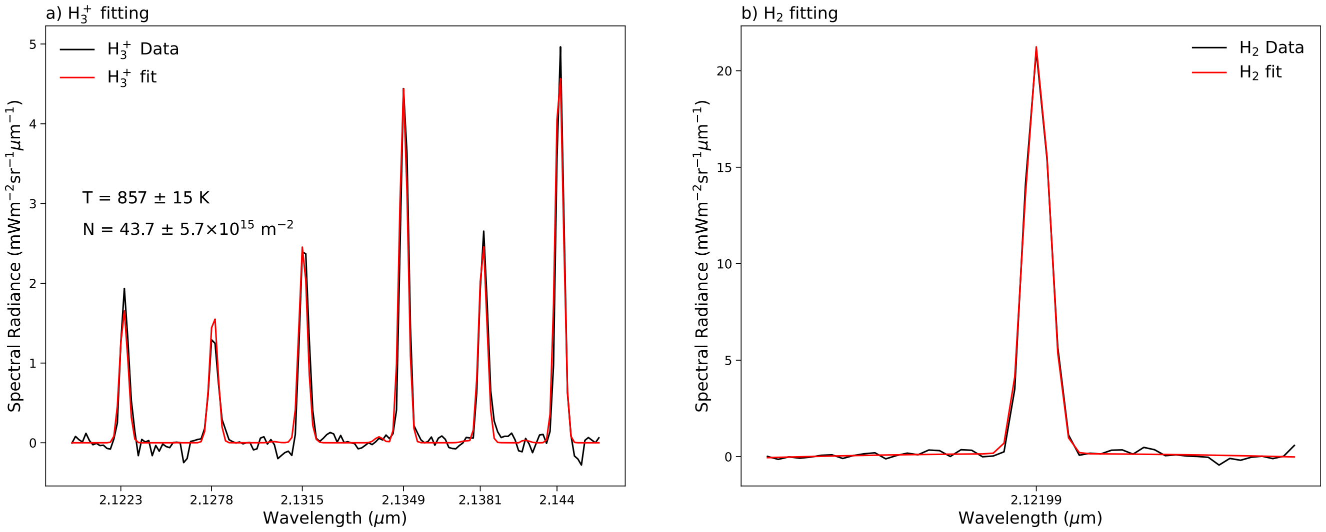

Figure 1. Example observed (a) H_3^+ and (b) H_2 spectra (black) with model fit (red). H_3^+ temperature and column density are retrieved with uncertainties.

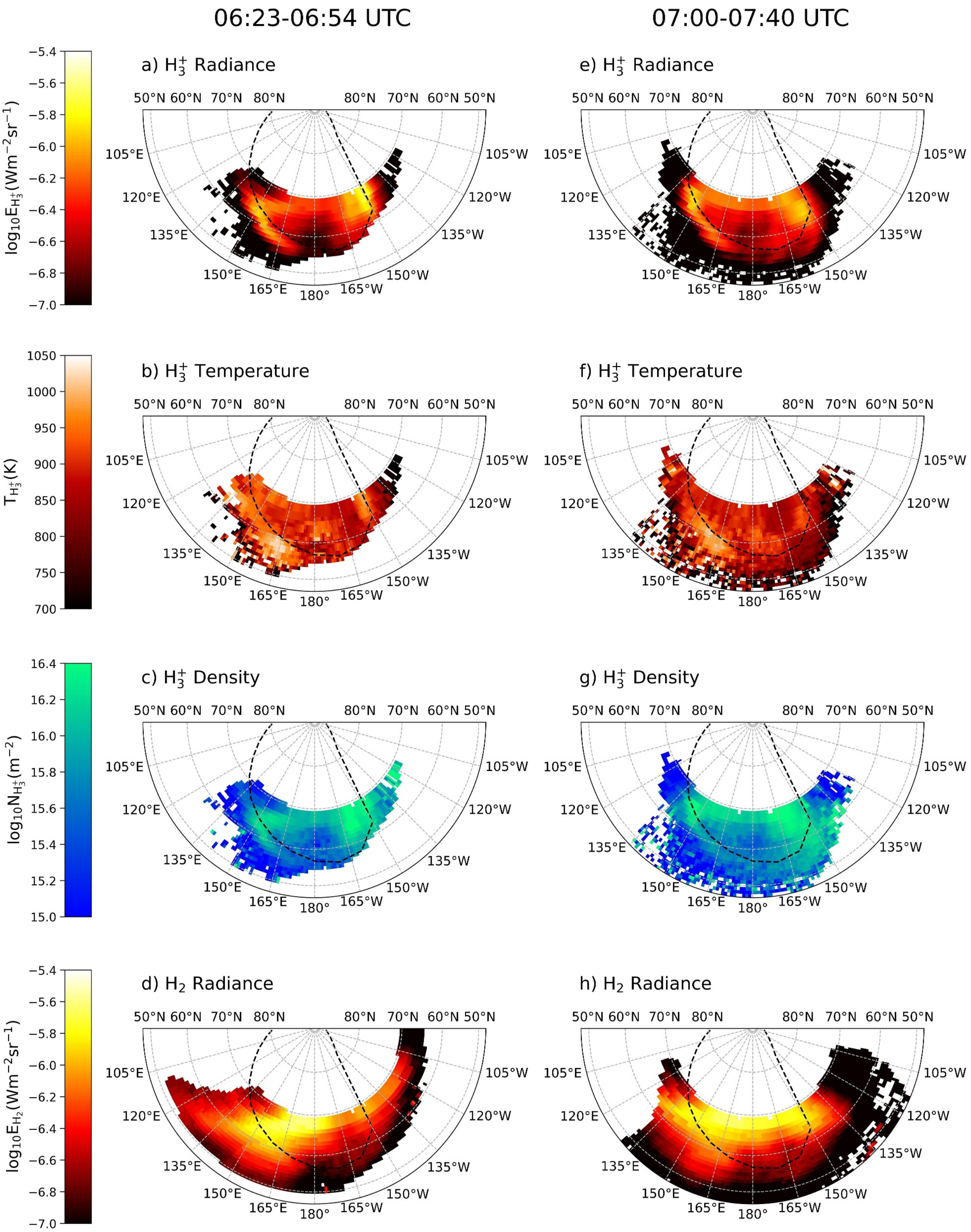

Figure 2. Polar projected maps of the measured H_3^+ (a, e) radiance, (b, f) temperature, and (c, g) column density, along with the H_2 (d, h) radiance. The time span of each scan taken on 02 June 2017 is shown at the top. The dashed black line marks the main emission of Jupiter's aurora, obtained from the model of Grodent et al. (2001).

cold spot near 65°N, 165°W. Raynaud et al. (2004) and Moore et al. (2017) reported similar temperature variations, though these structures appear to be highly versatile. We also identify a large area with lower temperature poleward of the main emission in the dawn polar region, which has been previously seen in Johnson et al. (2018).

The column densities of H_3^+ are shown in Figures 2c and 2g, with mean values of 8.05 and 7.97 $\times 10^{15}$ m^{-2}. Large densities are found along the two auroral peaks and in the polar region just below 70°N, whereas the region around ~65°N, 180° is notably less dense than the surroundings. The high-density region on the dusk side is expanded, with the peak offsets ~5° poleward of the dusk main emission. On the dawn side, the dense region becomes narrow and confined. Again, these results are similar to Moore et al. (2017), where the densities are found to be higher in the dusk polar region and along the dawn auroral peak. Johnson et al. (2018) also reported similar morphology, but their peak densities in the dusk sector aligned more closely to the main emission without clear offsets. The error bars of H_3^+ column densities in Raynaud et al. (2004) were too large to make a comparison. Note that an anticorrelation relationship exists between density and temperature, which has been previously reported in Melin et al. (2014).

H_2 radiance shown in Figures 2d and 2h are averaged to 0.51 and 0.42 $\mu Wm^{-2}sr^{-1}$, respectively. Regions with high radiance are found on the dawn side and across the polar region above 60°N, extended to the dusk side. Below 60°N, from ~170°E to ~160°W, the radiance significantly drops below the average, resulting in notable dark regions in both scans. Raynaud et al. (2004) derived the H_2 radiance from the same $S_1(1)$ line and also identified a similar bright region in the dawn sector of the northern hemisphere. Considering that the two observations were conducted with different instruments in a nearly two-decade gap, it might be possible that this large bright spot is due to a persistent phenomenon in the thermosphere. However, more studies involving polar mapping of directly measured H_2 radiance are needed to validate our speculation.

We have attempted to determine the rotational temperature and column density from the observed H_2 lines $S_1(1)$, $Q_1(1)$, and $Q_2(2)$, following the same method applied to the H_3^+ lines. However, $Q_1(1)$ cannot be separated from the adjacent absorption line and skyline, while $Q_2(2)$ lacks a sufficient S/N ratio. We cannot confirm whether the quantities derived using these two lines represent real thermospheric conditions or refer to any artifacts of the fitting process. H_2 temperature and density are not shown due to these concerns. Only $S_1(1)$ is available to derive the H_2 wind velocity (Wang et al., 2023) and radiance (Figures 2d and 2h).

The uncertainties of the measured quantities are mainly associated with instrumental effects, the signal-to-noise ratio of the spectra, and the fitting errors propagated throughout the calculations. Figure 3 shows the corresponding uncertainties of the polar projection maps. From top to bottom of the uncertainty map: Figures 3a and 3e for H_3^+ radiance, Figures 3b and 3f for H_3^+ temperature, Figures 3c and 3g for H_3^+ density, and Figures 3d and 3h for H_2 radiance. Variations in the uncertainties of H_3^+ and H_2 radiance depend on the quality of the data and the background noise. These are generally consistent throughout the map after data reduction and removal of the continuum disk. Regions poleward of the main auroral emission are associated with lower uncertainties for H_3^+ temperature, where the signals are significantly stronger than those of the subauroral regions. The uncertainty maps of H_3^+ column density for both scans are positively correlated with the main results, where the uncertainties are higher in the region of higher densities due to lower temperature. The H_3^+ radiance is driven both by temperature and density. Although the density is high, the temperature is the main driver of the radiance, keeping the signal-to-noise ratio comparatively low. The overall signal-to-noise ratio remains relatively consistent due to this reason.

4. Discussion

4.1. Correlations Between H_3^+ Radiance, Temperature, and Density

We have determined the correlations between derived H_3^+ parameters to investigate potential connections. Data points used in the calculations only include those with intensities larger than 0.1 $\mu Wm^{-2}sr^{-1}$ to ensure strong S/N ratios. Due to data limitation, the Pearson correlation coefficient can be computed for only the second scan, which yields 0.75 between radiance and column density, 0.38 between radiance and temperature, and −0.28 between column density and temperature. Figure 4 shows the scatter plots between each quantity.

Relatively strong and positive correlations are found between radiance and column density, as shown in Figure 4a. Such relations can also be seen from the morphological comparisons between Figures 2a, 2c and Figures 2e, 2g,

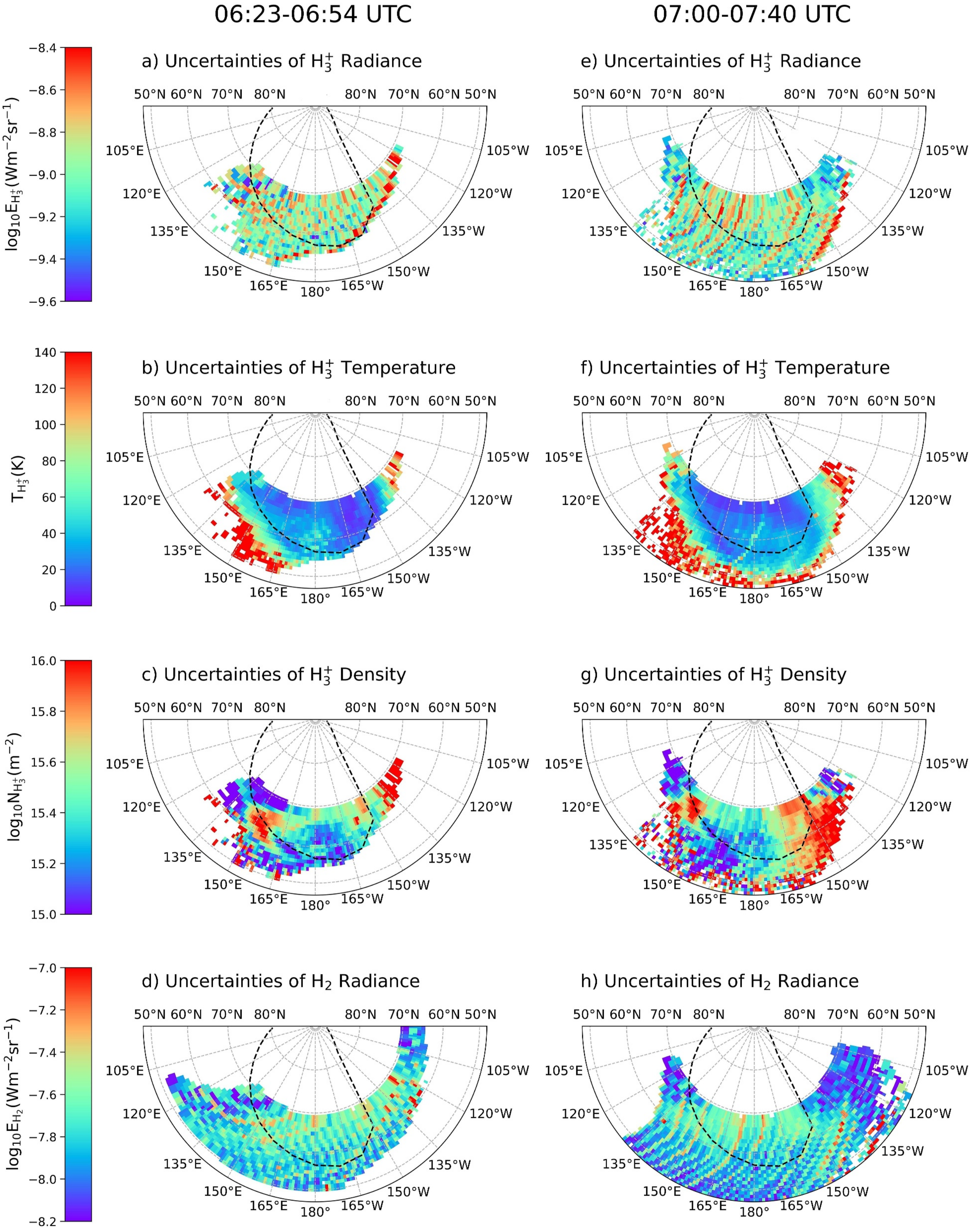

Figure 3. Uncertainties corresponding to the measured H_3^+ (a, e) radiance, (b, f) temperature, (c, g) column density, and H_2 (d, h) radiance. The plotting format is identical to Figure 2, except for the color bars.

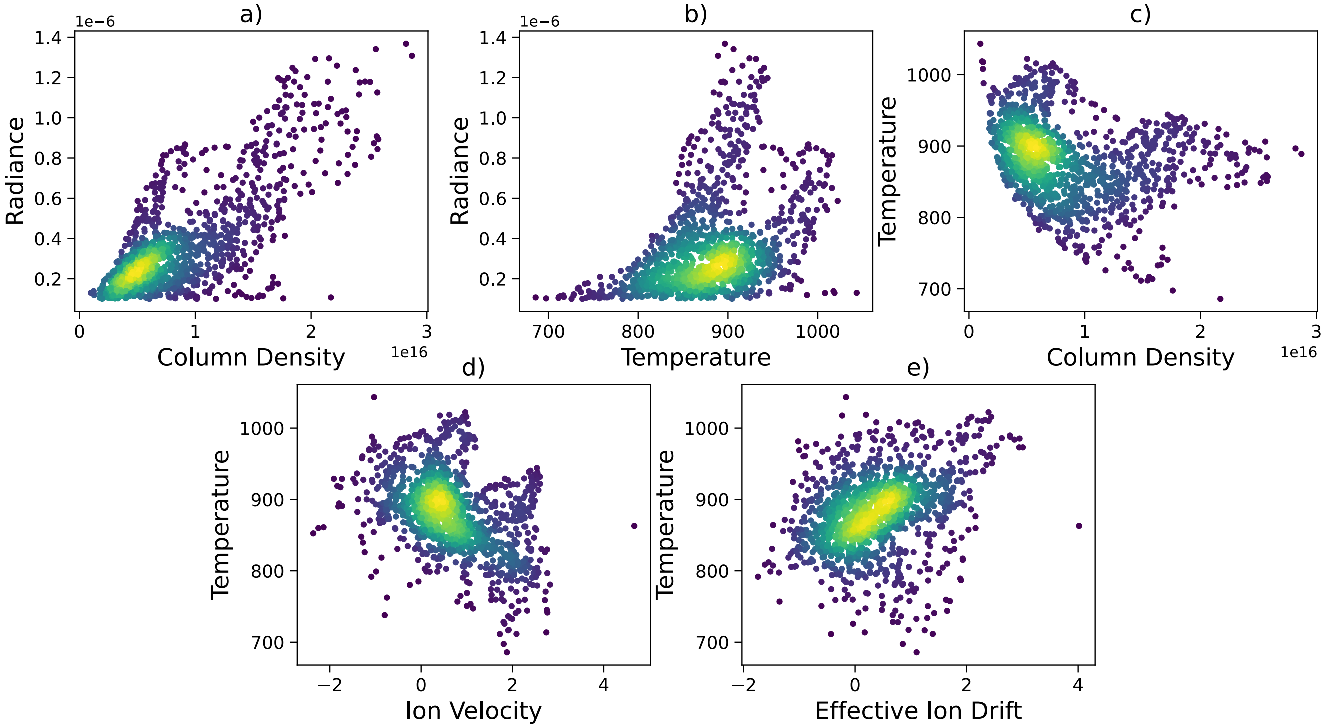

Figure 4. Scatter plots between (a) radiance and column density, (b) radiance and temperature, (c) temperature and column density, (d) temperature and ion wind velocity, and (e) temperature and effective ion drift. The velocities have been reported previously in Wang et al. (2023). A Gaussian kernel-density estimate is included in the colors to show the probability density of each variable. A lighter color represents a higher probability density, that is, a higher probability of occurrence of the event.

showing that regions with high radiance also have high densities, mainly along the auroral peaks and the polar region at 70°N. Positively correlated radiance and density have been reported in previous studies (e.g., Johnson et al., 2018; Moore et al., 2017; Stallard et al., 2002). Changes of H_3^+ radiance could result from variations in temperature, density, or a combination of both. Given that only the correlation between radiance and temperature is relatively lower, the density appears to be the more dominant driver of the emission intensity.

Correlations between the radiance and temperature of H_3^+ are difficult to quantify; Figure 4b reveals an unclear trend. Morphologically, when comparing Figures 2a and 2e with Figures 2b and 2f, regions such as 60°N, 165°E and 70°N, 150°W are found with enhanced temperature and radiance. On the other hand, at regions 65°N, 140°E, 65°N, 180°, and 65°N, 160°W, for example, temperature and radiance appear to be inversely correlated. Stallard et al. (2002) have seen such complex variations in the vibrational temperature derived from H_3^+ fundamental emission lines. Lystrup et al. (2008) later confirmed an anticorrelation between radiance and temperature determined from H_3^+ ion density profiles obtained using Keck-NIRSPEC.

The lack of correlation between radiance and temperature is not unexpected. Higher temperatures naturally occur higher in the atmosphere. However, the thermostat effect of H_3^+ provides cooling to the auroral region (Miller et al., 2000). At such high altitudes, densities are lower and, therefore, there is less gas, potentially less H_3^+, to radiate heat. As altitude increases, H_3^+ will be less thermally equilibrated, and individual H_3^+ molecule will thus radiate less efficiently (Miller et al., 2013). When a gas emits radiation from a planetary atmosphere, it inevitably produces a cooling effect that counters any warming caused by particle precipitation, EUV heating, chemical reactions, or conductive and mechanical heating, as indicated by Melin et al. (2006). The H_3^+ thermostat effect is most efficient when the gas is in LTE, but continues to function, although less effectively, even when the gas is not thermally equilibrated. At Jupiter, H_3^+ ions were predominantly produced in the main emission regions deeper within the atmosphere at around ~550 km (Melin et al., 2005). The H_3^+ thermostat effect is more effective in this region, so the temperature will decrease. The peak emission altitude of H_3^+ overtone emissions is at ~700 − 900 km (Kita et al., 2018; Uno et al., 2014), but the temperature measured in this work matches previous studies using

H_3^+ fundamental lines (Johnson et al., 2018; Moore et al., 2017), which implies that the heating for both layers may be driven by the same mechanism. The temperature of the emitting H_3^+ is affected by its vertical position in the atmosphere, the magnitude of electron precipitation energy, Joule heating, ion drag, and the degree to which the relevant H_3^+ ions are in LTE.

Figure 4c shows that the correlation between column density and temperature is modest and negative. Morphological comparisons between Figures 2b and 2c and 2f-g reveal that denser regions are generally colder, except near 60°N, 160°E and 65°N, 150°W. Potential anticorrelations between H_3^+ temperature and density have been reported in Lam et al. (1997) and Raynaud et al. (2004), although the uncertainties were too large to distinguish physical and statistical results. Such inverse correlations are expected to be seen in dense regions of H_3^+ with low temperature due to the H_3^+ thermostat effect (Miller et al., 2010). Moore et al. (2017) observed a cooling event of H_3^+ temperature alongside the increase of column density by comparing two different nights of ground-based observations separated by a 7-day gap. The temperature and density variations in their study were larger than the associated measurement uncertainties. Melin et al. (2014) has previously reported such an inverse relationship between density and temperature and attributed to an actual physical anticorrelation within Jupiter's atmosphere rather than artifacts of the fitting process. Adriani et al. (2017) showed that the auroral temperatures in the north and south differ significantly in both magnitude and behavior when compared in the local time, yet H_3^+ temperature still tended to be inversely proportional to the column density in the southern aurora. Energetic particle precipitation produces ionization in the upper atmosphere; a higher rate of ionization will produce more H_3^+ and thus increase the column density (Grodent et al., 2001). Johnson et al. (2018) reported a modest positive correlation between temperature and column density by comparing maps of H_3^+ parameters with high spatial resolution, which suggests dominant heating by particle precipitation. In a study of the observed auroral event by Stallard et al. (2001, 2002), Melin et al. (2006) modeled the auroral thermal balance based on observational data and showed that particle precipitation only contributes to a minor extent to the increase in temperature. Particle precipitation is likely to be highly variable in regulating the Jovian thermospheric temperature.

4.2. Correlations Between H_3^+ Temperature and Velocity

To investigate the effect of the interaction between Jupiter's upper atmosphere and magnetosphere, Johnson et al. (2018) measured the rotational temperature of H_3^+ and compared with the line-of-sight ion velocities in the planetary reference frame derived in Johnson et al. (2017), with the neutral atmosphere assumed in corotation with Jupiter. The authors found that the correlation between H_3^+ velocity and temperature was not strong. For the same comparison, we have transformed the line-of-sight H_3^+ ion wind velocity reported in Wang et al. (2023) from the observer reference frame to the planetary rotation frame by subtracting the rotation rate of Jupiter. Assuming that the thermosphere corotates with the planet, we compute a Pearson correlation coefficient of −0.40 between temperature and ion velocity, with a general trend of anticorrelation shown in Figure 4d, which is significantly different from Johnson et al. (2018) (~ 0.71). Structures of the ion velocity (Johnson et al., 2017; Wang et al., 2023) and ranges of the rotational temperature (Johnson et al., 2018 and Figures 2d and 2f) in both studies align well with each other and are consistent with past measurements (Chaufray et al., 2011; Moore et al., 2017; Stallard et al., 2001, 2002). The discrepancy may be caused by a departure from LTE due to altitudinal differences between H_3^+ fundamental and overtone emissions.

Giles et al. (2016) simultaneously measured the kinetic, rotational, and vibrational temperature using H_3^+ fundamental and overtone lines in the M band and found different values of each, suggesting a possible LTE breakdown. However, Stallard et al. (2002) reported positive correlations between vibrational temperature and ion velocities using H_3^+ fundamental and hot band emissions, consistent with the positive correlation between rotational temperature and H_3^+ velocities calculated in Johnson et al. (2018). The positive correlations noted in both studies suggest that, for H_3^+ fundamental emissions peaking at $\sim$550 km, a quasi-LTE appears to be valid, matching predictions by Melin et al. (2005) that H_3^+ fundamental emissions are least affected by the non-LTE effect. Tao et al. (2011) showed that the departure from LTE is not significant until above ~1,000 km. As a result, we consider that our assumption of quasi-LTE for H_3^+ overtone emissions ($\sim 700 - 900$ km; Uno et al., 2014; Kita et al., 2018) can be deemed reasonable; the difference between results in this study and in Johnson et al. (2018) is likely due to other reasons yet to be known. However, a rigorous study of the LTE effect is suggested to validate its impact at different altitudes in the upper atmospheres of giant planets.

Joule heating is the thermalized kinetic energy heating the atmosphere, resulting from the relative motion between ions and neutrals in the upper atmosphere (Smith et al., 2005). The magnitude of Joule heating is determined by several factors and one of them is the velocity difference between the neutrals and plasmas (small-scale fluctuations in electric fields may also affect the magnitude of Joule heating; Smith et al., 2005). In this particular case, we expect to see the largest Joule heating in regions where the difference between neutral and ion velocities is the largest. Significantly different spatial correlations in Johnson et al. (2018) and this study indicate that short-term observations can not reveal the full picture of the dynamical Jovian system with rapidly fluctuating inputs that drive strong temperature gradients.

By taking into account the subcorotational thermospheric wind, as shown in Figure 4e, a weak positive correlation has been found between the effective ion drift in Wang et al. (2023) and the H_3^+ rotational temperature measured in this study, with a Pearson correlation coefficient of 0.32. This is significantly different from the value calculated without considering the neutral motions. Such a correlation relation may be relevant to the ion drag energy in the heating of Jupiter's upper atmosphere. In addition to Joule heating, the relative motion between ions and neutrals in the upper atmosphere can also lead to ion drag, another component of heating due to the exchange of kinetic energy that provides considerable energy inputs to the upper atmosphere (Smith et al., 2005; Vasyliūnas & Song, 2005). However, it is still not yet clear whether these two components should be discussed separately.

Most previous models have treated Joule heating and ion drag as a whole. Smith and Aylward (2009) predicted the occurrence of maximum Joule heating and ion drag at the peak Pedersen conductivity layer, where the ion-neutral collision frequency equals the ion gyrofrequency; the altitude of this layer has been modeled to peak near 500 km (Tao et al., 2011). Melin et al. (2006) showed that Joule heating and ion drag deposit energy at the altitude of peak H_3^+ ion density, corresponding to the altitude of peak Pedersen conductivity. Calculated based on Tao et al. (2009), Wang et al. (2023) showed that ion drag is only a weak term at depth but dominates the accelerating force compared to all the forces that affect the neutral atmosphere in and above the main ionospheric region (>400 km). The effective ion drifts measured from H_3^+ overtone emissions were predicted to broadly represent the effective ion flows between $\sim 400 - 600$ km. The overlap altitude at ~ 500 km suggests that the impact of Joule heating and ion drag to the temperature variations at the peak layer of H_3^+ fundamental emission are highly likely linked to the neutral thermosphere as predicted. Simulations by Yates et al. (2020) suggested that subcorotating neutral flows would lead to smaller Pedersen currents in the ionosphere and thus decrease Joule heating and ion drag. The weak positive correlation shown in Figure 4e may be an indicator of such a modeled case. Future models are thus suggested to include the effect of neutral thermospheric winds, as well as separate inputs of Joule heating and ion drag energy.

Deep in the lower atmosphere, Sinclair et al. (2017) reported an increase in temperature in the northern auroral region of Jupiter's stratosphere at an altitude corresponding to a pressure of ~ 10 μbar, below the stratosphere–thermosphere boundary (~ 360 km or ~ 0.34 μbar; Seiff et al., 1998). The authors proposed that the heating may be due to heat conducted from higher thermospheric altitudes, involving the interaction of downward precipitated electrons with molecules in the upper atmosphere, Joule heating, ion drag, and energy released from exothermic chemical reactions of ions. Yates et al. (2020) reported a negative vertical temperature gradient above ~ 500 km in their model and argued that this could be due to the model not including energy sources at high altitudes. Although the temperature measured in this study is derived from the H_3^+ overtone emissions located at a much higher altitude ($\sim 700 - 900$ km; Kita et al., 2018; Uno et al., 2014), the value of the temperature is still highly comparable to the results reported in previous studies (Johnson et al., 2018; Moore et al., 2017), which were derived from the H_3^+ fundamental emissions (~ 550 km; Melin et al., 2005) Majeed et al. (2009) modeled the vertical profile of heating in Jupiter's auroral region and noticed a heating event dominated by ion drag in the northern auroral oval between 0.2 and 0.01 μbar. These pressures correspond to altitudes higher than the stratosphere–thermosphere boundary. It is possible that the source of thermospheric heating originates from an altitude above the stratosphere but below the peak layer of H_3^+ overtone emissions, releasing heat to the surrounding regions and altitudes above and below. Verification of these speculations would need direct observations of Jupiter's thermosphere. The limitations of ground-based infrared observations of H_2 quadrupole emission reported in our study may be overcome using the upgraded Keck-NIRSPEC (Martin et al., 2018), potentially benefiting future work to decipher the unknown mechanism behind the high Jovian thermospheric temperature.

5. Conclusions

We have observed H_2 quadrupole and H_3^+ overtone emissions simultaneously in Jupiter's northern auroral zone on 02 June 2017 using Keck-NIRSPEC and present high-resolution polar maps of H_3^+ radiance, rotational temperature, column density, and H_2 radiance. Although there are slight structural differences, the derived parameters of H_3^+ and H_2 share broad similarities with those measured in previous observations Raynaud et al. (2004), Moore et al. (2017), Johnson et al. (2018). We have compared these physical quantities to search for potential correlations with known auroral heating sources such as particle precipitation, Joule heating, and ion drag. Additionally, we have compared the temperature with ion wind velocity in the context of Jupiter's rotation rate and the neutral wind velocity previously reported in Wang et al. (2023). H_3^+ radiance generally reveals a strong correlation with density but is not highly correlated with temperature, while a weak anticorrelation has been found between density and temperature. Between H_3^+ temperature and ion velocity, there is a negative correlation when neutral velocities are not considered and a positive correlation after taking into account the thermospheric wind. It is unclear whether a single dominant heating mechanism is responsible for Jupiter's auroral thermospheric heating. The results suggest a complex interaction between heating by a combination of multiple drivers and cooling due to the H_3^+ thermostat effect. The dependence of the temperature of the emitting H_3^+ on its vertical position in the atmosphere has also been discussed. The level of H_3^+ ions under the LTE effect may be of significance to the thermospheric heating in Jupiter. Comparisons with previously observed auroral heating events deep in Jupiter's stratosphere (Sinclair et al., 2017) and models of vertical temperature profiles (Majeed et al., 2009; Yates et al., 2020) suggest that the heat source may originate from an altitude between the stratosphere and peak layer of H_3^+ overtone and H_2 quadrupole emissions. Simultaneous observations of both H_3^+ and H_2 with improved instruments could potentially resolve more details of structure variability, especially with direct measurements of H_2 thermospheric temperature. With a full investigation of the LTE effect, the driver of heating may be further understood.

Acknowledgments

This work was supported by a NASA Keck PI Data Award, administered by the NASA Exoplanet Science Institute. Data presented herein were obtained at the W. M. Keck Observatory from telescope time allocated to the National Aeronautics and Space Administration through the agency's scientific partnership with the California Institute of Technology and the University of California. The Observatory was made possible by the generous financial support of the W. M. Keck Foundation. The authors wish to recognize and acknowledge the very significant cultural role and reverence that the summit of Maunakea has always had within the indigenous Hawaiian community. We are most fortunate to have the opportunity to conduct observations from this mountain. A portion of this research was carried out at the Jet Propulsion Laboratory, California Institute of Technology, under a contract with the National Aeronautics and Space Administration. RW was supported by a University of Leicester Doctoral Scholarship. TS was supported by the UK Science and Technology Facilities Council (STFC) Consolidated Grant ST/W00089X/1. HM was supported by the STFC James Webb Fellowship ST/W001527/1 at the University of Leicester. LM was supported by Grant 80NSSC20K1045 issued through the NASA Solar System Workings program. JOD was supported by the STFC Ernest Rutherford Fellowship. KK was supported by a Northumbria University Doctoral Scholarship. PT was supported by the STFC Studentship Grant ST/X508548/1. Ruoyan Wang genuinely thanks Huiyuqing Liu for the invalubale care and mental support over the years.

Data Availability Statement

The data used in this study are publicly available at the Keck Observatory Archive (KOA, http://koa.ipac.caltech.edu/cgi-bin/KOA/nph-KOAlogin), which is operated by the W. M. Keck Observatory and the NASA Exoplanet Science Institute (NExScI), under contract with the National Aeronautics and Space Administration.

References

Adriani, A., Mura, A., Moriconi, M. L., Dinelli, B. M., Fabiano, F., Altieri, F., et al. (2017). Preliminary JIRAM results from Juno polar observations: 2. Analysis of the Jupiter southern $H_3{}^+$ emissions and comparison with the north aurora. *Geophysical Research Letters*, *44*(10), 4633–4640. https://doi.org/10.1002/2017GL072905

Chaufray, J. Y., Greathouse, T. K., Gladstone, G. R., Waite, J. H., Maillard, J. P., Majeed, T., et al. (2011). Spectro-imaging observations of Jupiter's 2 μm auroral emission. II: Thermospheric winds. *Icarus*, *211*(2), 1233–1241. https://doi.org/10.1016/j.icarus.2010.11.021

Drossart, P., Maillard, J. P., Caldwell, J., Kim, S. J., Watson, J. K. G., Majewski, W. A., et al. (1989). Detection of $H_3{}^+$ on Jupiter. *Nature*, *340*(6234), 539–541. https://doi.org/10.1038/340539a0

Giles, R. S., Fletcher, L. N., Irwin, P. G. J., Melin, H., & Stallard, T. S. (2016). Detection of $H_3{}^+$ auroral emission in Jupiter's 5-micron window. *Astronomy and Astrophysics*, *589*, A67. https://doi.org/10.1051/0004-6361/201628170

Grodent, D., Waite, J., Hunter, J., & Gérard, J.-C. (2001). A self-consistent model of the Jovian auroral thermal structure. *Journal of Geophysical Research*, *106*(A7), 12933–12952. https://doi.org/10.1029/2000JA900129

Johnson, R. E., Melin, H., Stallard, T. S., Tao, C., Nichols, J. D., & Chowdhury, M. N. (2018). Mapping $H_3{}^+$ temperatures in Jupiter's northern auroral ionosphere using VLT-CRIRES. *Journal of Geophysical Research (Space Physics)*, *123*(7), 5990–6008. https://doi.org/10.1029/2018JA025511

Johnson, R. E., Stallard, T. S., Melin, H., Nichols, J. D., & Cowley, S. W. H. (2017). Jupiter's polar ionospheric flows: High resolution mapping of spectral intensity and line-of-sight velocity of $H_3{}^+$ ions. *Journal of Geophysical Research (Space Physics)*, *122*(7), 7599–7618. https://doi.org/10.1002/2017JA024176

Kim, S., Drossart, P., Caldwell, J., & Maillard, J. P. (1990). Temperatures of the Jovian auroral zone inferred from 2-μm H_2 quadropole line observations. *Icarus*, *84*(1), 54–61. https://doi.org/10.1016/0019-1035(90)90157-5

Kita, H., Fujisawa, S., Tao, C., Kagitani, M., Sakanoi, T., & Kasaba, Y. (2018). Horizontal and vertical structures of Jovian infrared aurora: Observation using Subaru IRCS with adaptive optics. *Icarus*, *313*, 93–106. https://doi.org/10.1016/j.icarus.2018.05.002

Lam, H. A., Achilleos, N., Miller, S., Tennyson, J., Trafton, L. M., Geballe, T. R., & Ballester, G. E. (1997). A baseline spectroscopic study of the infrared auroras of Jupiter. *Icarus*, *127*(2), 379–393. https://doi.org/10.1006/icar.1997.5698

Lystrup, M. B., Miller, S., Dello Russo, N., Vervack, J. R. J., & Stallard, T. (2008). First vertical ion density profile in Jupiter's auroral atmosphere: Direct observations using the Keck II telescope. *The Astrophysical Journal*, *677*(1), 790–797. https://doi.org/10.1086/529509

Majeed, T., Waite, J. H., Bougher, S. W., & Gladstone, G. R. (2009). Processes of auroral thermal structure at Jupiter: Analysis of multispectral temperature observations with the Jupiter thermosphere general circulation model. *Journal of Geophysical Research (Planets)*, *114*(E7), E07005. https://doi.org/10.1029/2008JE003194

Martin, E. C., Fitzgerald, M. P., McLean, I. S., Doppmann, G., Kassis, M., Aliado, T., et al. (2018). An overview of the NIRSPEC upgrade for the Keck II telescope. In C. J. Evans, L. Simard, & H. Takami (Eds.), *Ground-based and airborne instrumentation for astronomy VII* (Vol. 10702, p. 107020A). https://doi.org/10.1117/12.2312266

Melin, H., Miller, S., Stallard, T., & Grodent, D. (2005). Non-LTE effects on H_3^+ emission in the Jovian upper atmosphere. *Icarus*, *178*(1), 97–103. https://doi.org/10.1016/j.icarus.2005.04.016

Melin, H., Miller, S., Stallard, T., Smith, C., & Grodent, D. (2006). Estimated energy balance in the Jovian upper atmosphere during an auroral heating event. *Icarus*, *181*(1), 256–265. https://doi.org/10.1016/j.icarus.2005.11.004

Melin, H., Stallard, T. S., O'Donoghue, J., Badman, S. V., Miller, S., & Blake, J. S. D. (2014). On the anticorrelation between H_3+ˆtemperature and density in giant planet ionospheres. *Monthly Notices of the Royal Astronomical Society*, *438*(2), 1611–1617. https://doi.org/10.1093/mnras/stt2299

Miller, S., Achilleos, N., Ballester, G. E., Geballe, T. R., Joseph, R. D., Prangé, R., & Waite, J. J. H. (2000). The role of H_3^+ in planetary atmospheres. In *Astronomy, physics and chemistry of* h_3^+ (Vol. 358, pp. 2359–2559). https://doi.org/10.1098/rsta.2000.0662

Miller, S., Stallard, T., Melin, H., & Tennyson, J. (2010). H3+ cooling in planetary atmospheres. *Faraday Discussions*, *147*, 283. https://doi.org/10.1039/c004152c

Miller, S., Stallard, T., Tennyson, J., & Melin, H. (2013). Cooling by H3+ emission. *Journal of Physical Chemistry A*, *117*(39), 9770–9777. https://doi.org/10.1021/jp312468b

Miller, S., Tennyson, J., Geballe, T. R., & Stallard, T. (2020). Thirty years of H_3^+ astronomy. *Reviews of Modern Physics*, *92*(3), 035003. https://doi.org/10.1103/RevModPhys.92.035003

Millward, G., Miller, S., Stallard, T., Achilleos, N., & Aylward, A. D. (2005). On the dynamics of the Jovian ionosphere and thermosphere. IV. Ion-neutral coupling. *Icarus*, *173*(1), 200–211. https://doi.org/10.1016/j.icarus.2004.07.027

Moore, L., O'Donoghue, J., Melin, H., Stallard, T., Tao, C., Zieger, B., et al. (2017). Variability of Jupiter's IR H_3^+ aurorae during Juno approach. *Geophysical Research Letters*, *44*(10), 4513–4522. https://doi.org/10.1002/2017GL073156

Neale, L., Miller, S., & Tennyson, J. (1996). Spectroscopic properties of the H_3^+ molecule: A new calculated line list. *The Astrophysical Journal*, *464*, 516. https://doi.org/10.1086/177341

O'Donoghue, J., Moore, L., Bhakyapaibul, T., Melin, H., Stallard, T., Connerney, J. E. P., & Tao, C. (2021). Global upper-atmospheric heating on Jupiter by the polar aurorae. *Nature*, *596*(7870), 54–57. https://doi.org/10.1038/s41586-021-03706-w

Raynaud, E., Lellouch, E., Maillard, J. P., Gladstone, G. R., Waite, J. H., Bézard, B., et al. (2004). Spectro-imaging observations of Jupiter's 2μm auroral emission. I. H_3^+ distribution and temperature. *Icarus*, *171*(1), 133–152. https://doi.org/10.1016/j.icarus.2004.04.020

Roueff, E., Abgrall, H., Czachorowski, P., Pachucki, K., Puchalski, M., & Komasa, J. (2019). The full infrared spectrum of molecular hydrogen. *Astronomy & Astrophysics*, *630*, A58. https://doi.org/10.1051/0004-6361/201936249

Seiff, A., Kirk, D. B., Knight, T. C. D., Young, R. E., Mihalov, J. D., Young, L. A., et al. (1998). Thermal structure of Jupiter's atmosphere near the edge of a 5-μm hot spot in the north equatorial belt. *Journal of Geophysical Research*, *103*(E10), 22857–22890. https://doi.org/10.1029/98JE01766

Sinclair, J. A., Orton, G. S., Greathouse, T. K., Fletcher, L. N., Moses, J. I., Hue, V., & Irwin, P. G. J. (2017). Jupiter's auroral-related stratospheric heating and chemistry I: Analysis of Voyager-IRIS and Cassini-CIRS spectra. *Icarus*, *292*, 182–207. https://doi.org/10.1016/j.icarus.2016.12.033

Smith, C. G. A., & Aylward, A. D. (2009). Coupled rotational dynamics of Jupiter's thermosphere and magnetosphere. *Annales Geophysicae*, *27*(1), 199–230. https://doi.org/10.5194/angeo-27-199-2009

Smith, C. G. A., Miller, S., & Aylward, A. D. (2005). Magnetospheric energy inputs into the upper atmospheres of the giant planets. *Annales Geophysicae*, *23*(5), 1943–1947. https://doi.org/10.5194/angeo-23-1943-2005

Stallard, T., Miller, S., Millward, G., & Joseph, R. D. (2001). On the dynamics of the Jovian ionosphere and thermosphere. I. The measurement of ion winds. *Icarus*, *154*(2), 475–491. https://doi.org/10.1006/icar.2001.6681

Stallard, T., Miller, S., Millward, G., & Joseph, R. D. (2002). On the dynamics of the Jovian ionosphere and thermosphere. II. The measurement of H_3^+ vibrational temperature, column density, and total emission. *Icarus*, *156*(2), 498–514. https://doi.org/10.1006/icar.2001.6793

Tao, C., Badman, S. V., & Fujimoto, M. (2011). UV and IR auroral emission model for the outer planets: Jupiter and Saturn comparison. *Icarus*, *213*(2), 581–592. https://doi.org/10.1016/j.icarus.2011.04.001

Tao, C., Fujiwara, H., & Kasaba, Y. (2009). Neutral wind control of the Jovian magnetosphere-ionosphere current system. *Journal of Geophysical Research (Space Physics)*, *114*(A8), A08307. https://doi.org/10.1029/2008JA013966

Trafton, L., Lester, D. F., & Thompson, K. L. (1989). Unidentified emission lines in Jupiter's northern and southern 2 micron aurorae. *The Astrophysical Journal Letters*, *343*, L73. https://doi.org/10.1086/185514

Uno, T., Kasaba, Y., Tao, C., Sakanoi, T., Kagitani, M., Fujisawa, S., et al. (2014). Vertical emissivity profiles of Jupiter's northern H_3^+ and H_2 infrared auroras observed by Subaru/IRCS. *Journal of Geophysical Research (Space Physics)*, *119*(12), 10219–10241. https://doi.org/10.1002/2014JA020454

Vasyliūnas, V. M., & Song, P. (2005). Meaning of ionospheric Joule heating. *Journal of Geophysical Research (Space Physics)*, *110*(A2), A02301. https://doi.org/10.1029/2004JA010615

Wang, R., Stallard, T. S., Melin, H., Baines, K. H., Achilleos, N., Rymer, A. M., et al. (2023). Asymmetric ionospheric jets in Jupiter's aurora. *Journal of Geophysical Research (Space Physics)*, *128*(12), e2023JA031861. https://doi.org/10.1029/2023JA031861

Yates, J. N., Ray, L. C., Achilleos, N., Witasse, O., & Altobelli, N. (2020). Magnetosphere-ionosphere-thermosphere coupling at Jupiter using a three-dimensional atmospheric general circulation model. *Journal of Geophysical Research (Space Physics)*, *125*(1), e26792. https://doi.org/10.1029/2019JA026792

Yelle, R. V., & Miller, S. (2004). Jupiter's thermosphere and ionosphere. In F. Bagenal, T. E. Dowling, & W. B. McKinnon (Eds.), *Jupiter. The planet, satellites and magnetosphere* (Vol. 1, pp. 185–218).